12/31/2023
Part II

Experimental-Computational Analysis of Multi-inlet SCPP

Solar chimney power plant systems (SCPPS) offer a simple and reliable way to generate electricity using solar radiation to drive a flow of buoyant air. A typi-cal SCPP setup includes a collector, a tower, and a turbine or several turbines. Current SCPP designs have low thermal efficiency: only between 0.5% and 5%of the incident solar energy is converted into electricity. Inefficiencies result par-tially from limited mass flow rates through the tower. It is therefore desirable to provide a new design for the collector to increase the inlet air mass flow rate. In this paper, we present a double-inlet collector concept and results of numerical analysis to evaluate this design in terms of flow rate improvement. Computational fluid dynamics (CFD) was utilized to perform the numerical modeling and simulation (MS) by using a finite volume method package. The Manzanares prototype (the only operational solar tower power plant with available published reports) is selected to implement the double-inlet collector design and study its effect on the power plant. Beside this case, we fabricated a 1/1000 scale model of the Manzanares prototype which enables us to measure the field variables experimentally. Validation analysis was performed to quantify the reliability of our numerical model with respect to the available experimental data. We obtained a significant increase (14%) in the available output power by using the double-inlet collector.

Nomenclature

$Variables$

A cross-sectional area, m^2

A_r cross-sectional area of the collector ground, m^2

g acceleration due to gravity, m/s^2

h height, m

$\dot{m}$ air mass flow rate, kg/s

p pressure, N/m^2

$\dot{W}$ flow power, W

q heat transfer per unit mass, J/kg

q'' heat flux, W/m^2

R air specific gas constant, $J/kg.K$

T temperature,K

ρ density, kg/m^3

u velocity, m/s

c_p specific heat capacity, $J/kg.K$

D experimental data

S simulation result

Subscripts

i inlet

o outlet

c collector

t tower

m mean

∞ ambient air

$turb$ turbine

atm atmospheric

Abbreviations

CFD computational fluid dynamics

EOS equation of state

IGV inlet guide vanes

$M\&S$ modeling and simulation

PIV particle image velocimetry

RHS right hand side

$SCPPS$ solar chimney power plant system

1 Introduction

Solar energy is one of the promising renewable energy sources, as the annual amount of energy sufficient for the needs of our civilization is delivered to Earth by the Sun in only one hour [1]. Therefore, developing new technologies which can harvest solar energy efficiently is a prime importance. One of these technologies is solar chimney power plants (SCPP) which not only provide electricity on a large scale but also increase the chance of precipitation, even in low-humidity desert regions, and support the agriculture around the SCPP. In a solar chimney plant, the energy of buoyant hot air is converted to electrical energy. The plant consists of a collector at the base covered with a transparent roof that collects the solar radiation, heating the air inside and the ground underneath. In the center of the collector, there is a tower, and a turbine is located at its base. The hot air flows up the tower as a result of its buoyancy, and its energy is extracted and converted to electricity with the turbine. A typical solar chimney is shown in Fig. 2.1 .

Since the efficiency of SCPP as sketched is relatively low, for commercial SCPP the chimney and collector need to be built on a very large scale which results in

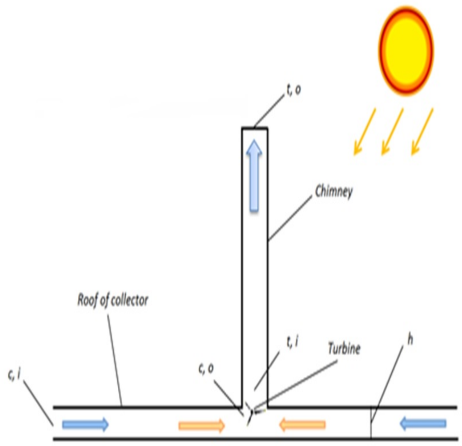

FIGURE 2.1: Schematic of a solar chimney power plant

high capital cost. Therefore any improvement in efficiency that leads to fabrication of smaller and less expensive SCPP can make the output electricity more competitive. Toward this end, since the successful construction and operation of Manzanares prototype in 1982 [2], considerable research efforts have been undertaken to improve the efficiency of SCPP and advance our knowledge in this area. An analytical and numerical study describes the influence of the chimney height, collector area, and pressure drop factor at the turbine on the output power of SCPP [3]. The output power was found to be proportional to the volume included within the chimney height and the collector area. In an effort to improve the efficiency of the collector and reduce its fabrication cost, Bonnelle [4] proposed a collector with ribs containing their branching. This concept provides larger entrance area, smaller air velocity, and lower friction under a lower roof compared with the conventional collector for the same flow rate. Bernardes et al. [5] analyzed the horizontal to vertical flow passage from the collector to the chimney for various designs including straight, curved, slanted junctions, and a conic chimney.

It was observed that the conic chimney had a higher mass flow rate and temperature at the outlet while the straight junction gave the smallest flow rate due to the occurrence of recirculation. During night time, as there is no solar energy to heat up the air, the only source of energy is the heated soil under the collector, which may not be sufficient for effective operation of SCPP. To address this issue various solutions such as inclusion of closed water-filled thermal storage system on the collector ground [6], usage of waste heat from nuclear power plants [7], and inclusion of an intermediate secondary roof under the first collector roof [8] have been suggested. In the latter design, the collector is divided into a top and bottom section. In the top section the air flows constantly, while in the bottom section the air flow can be regulated to store the energy during the day and release it at night [8]. It is widely known that, based on Betz's law [9], the maximum possible power that can be extracted by a free-standing wind turbine is limited to 59% of the kinetic energy of the wind. For a ducted turbine (as in the SCPP), 75% to 85% of the flow energy can be extracted, taking into account losses associated with conversion from mechanical to electrical energy [10]. In other recent works, the SCPPS design involving an inflatable tower was evaluated experimentally and numerically and validation assessment was performed for a small prototype [11, 12]. Various turbine configurations have been proposed to replace the conventional single vertical axis turbine. The multiple vertical axis and the multiple horizontal axis turbine configurations are among them [13, 14]. Fluri and von Backström [14] found that the single vertical axis turbine had a slightly higher efficiency and energy yield compared to the layouts with multiple axis turbines, as certain loss mechanisms were not present in the former. However, studies revealed that the peak output torques were considerably lower in the configurations with multiple turbines which may reduce the cost, particularly for the generators. In addition, the effects of inlet guide vanes (IGV) and counter-rotating rotors on the performance of the turbines have been studied [15, 16]. It was found that the counter-rotating turbines without IGV had lower design efficiency but higher off-design performance over a single-rotor turbine [15]. In this investigation, we propose a new conceptual design of a double-inlet collector for SCPPS. We study the change of output power of the power plant due to implementation of this design, and compare its performance with that of a traditional collector.

2 Conceptual Design

Our idea is to consider more than one inlet for the SCPPS collector. This novel design is a part of a pending patent [17]. Until now, none of the SCPPS collectors have been built with more than one inlet. Having the secondary inlet can increase the total inlet air mass flow rate which leads to a higher harvestable kinetic energy for the turbine to produce electricity. Fig. 2.2 presents the traditional (case A) and proposed double-inlet collector (case B) schematically.

3 Modeling and Simulation Approach

To evaluate the effect of having an extra inlet in the collector on the overall power plant performance, we modeled case B using ANSYS modeling package based on

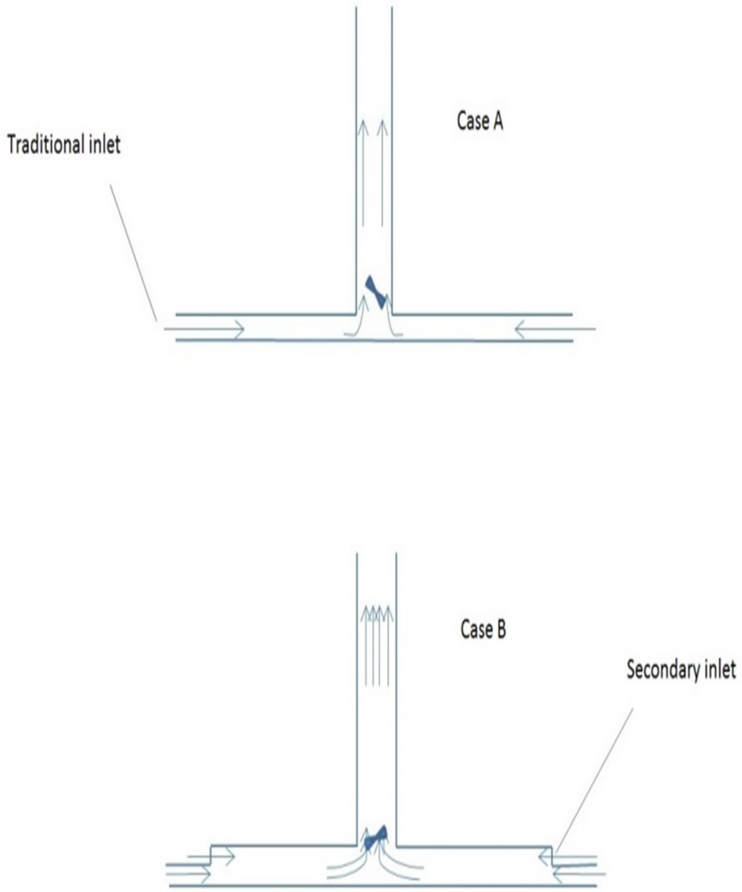

FIGURE 2.2: Schematic case description, traditional collector (Case A), double-inlet collector (Case B)

Manzanares prototype (Fig. 2.3). Numerical analysis was performed for both cases A and B to compare the traditional collector with the double-inlet collector for a range of solar radiation values, which is the available heat flux from the collector ground to air in our model.

To model and simulate the turbulent air flow, $k - \epsilon$ model in the commercial flow solver, ANSYS/FLUENT 17.1, was selected. Steady state axisymmetric computational domain was created (Fig. 2.4). The grid generation tool in ANSYS/-Workbench was used to create the mesh in the fluid domain. An unstructured mesh consisting of quadrilaterals cells was generated for the entire domain. With respect to the sensitivity of pressure value to the air density and buoyancy effect in this model, density was calculated by applying equations of state (EOS).

Computational studies were performed on a 16-core AMD Opteron, 32 Gb Ram workstation. The applied boundary conditions for this axisymmetric model are shown in Fig. 4 as well. CFD calculations were performed with second order formal accuracy for all field variables. The residual convergence tolerance was set not to exceed 10^{-7}. Residuals were observed decreasing gradually with each iteration. The iteration error was calculated for the mass flow rate. In Eq. (2.1) index i represent the ith iteration in the CFD steady state calculation.

$$e_{\dot{m}_i} \equiv |\frac{\dot{m}_{converged} - \dot{m}_i}{\dot{m}_{converged}}| (2.1)$$

4 Analytical Approach

Recently comparative analytical modeling of a traditional collector of SCPP with available experimental values was performed [18]. To calculate the pressure difference generated at the collector and tower, we used the modified version of the above-mentioned analytical model. This analytical correlation uses a one-dimensional approach to mass, momentum and energy conservation equations. Air density was assumed to be related to pressure and temperature via EOS.

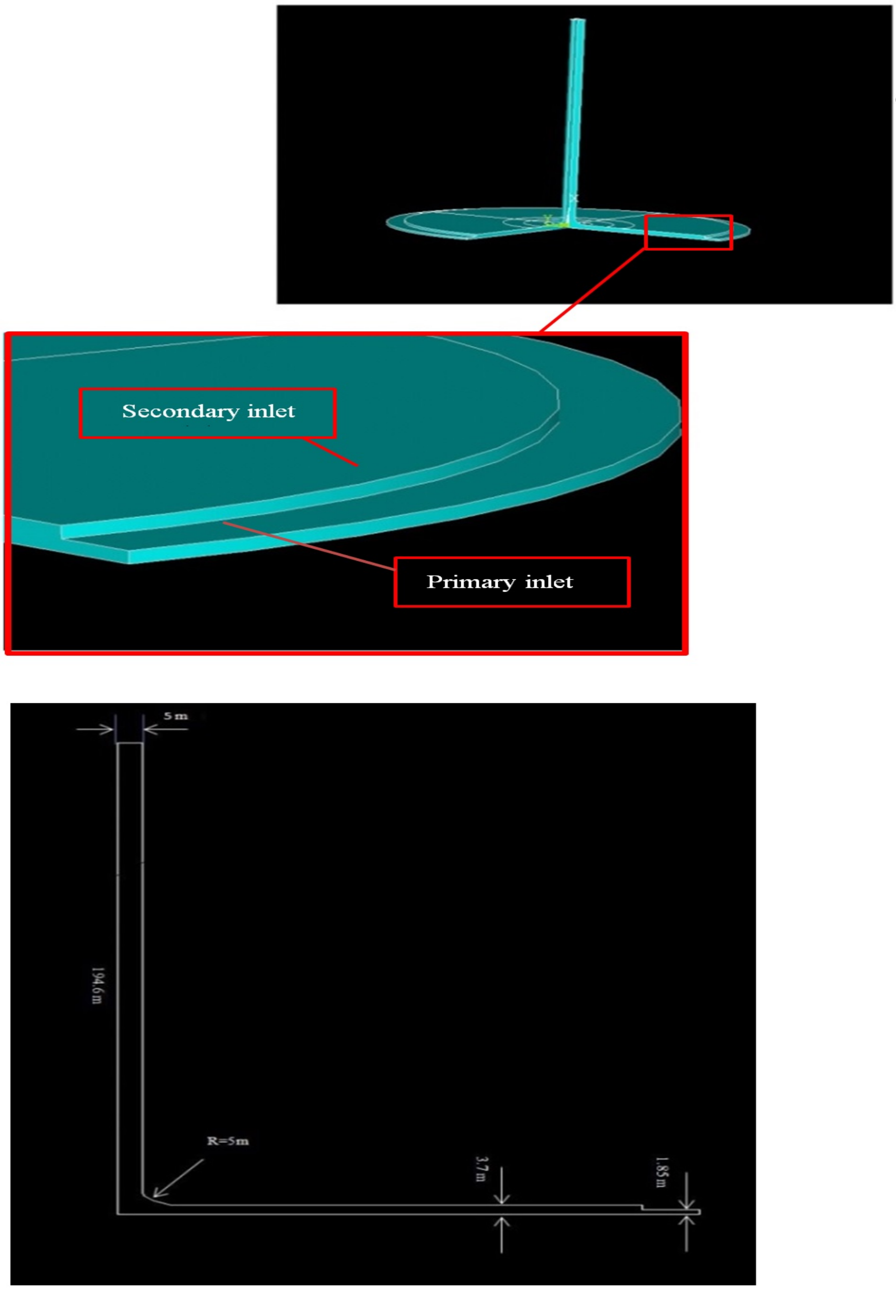

FIGURE 2.3: Case B model details

4.1 Collector

Solar Chimney Power Plants provide a reliable and conceptually straightforward way of energy generation from the solar irradiation[14, 17]. A solar collector is the main and only component of this power plant to accumulate the available solar

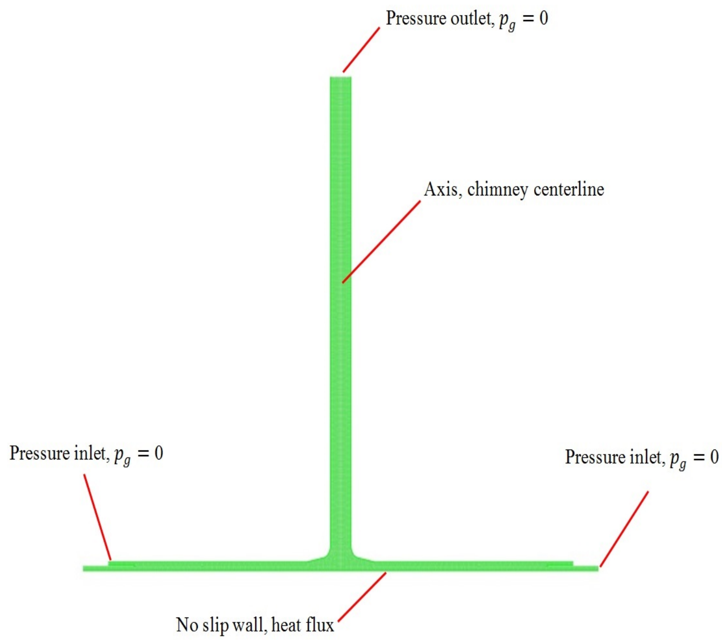

FIGURE 2.4: Computational domain of case B with the applied boundary conditions

energy to heat up air in a greenhouse. The air escapes the collector through a tall chimney which connects the warm air flow of the collector with the cooler air above the ground. The temperature difference induces the natural convection, and turbine at the outlet of collector harvests the energy of the air flow. To model the collector, the simplified one dimensional mathematical analysis was performed to clarify the details. The analytical correlation will be applied later to compare the CFD results against it. To derive the equations, we start from the collector. It is assumed that the flow through the collector is one-dimensional, steady-state, and compressible. Let us disregard the friction and assume the total heat from the solar irradiation is absorbed within the air filling the collector. For this thermal-fluid analysis, the mass conservation satisfies:

$$\frac{dA}{A} + \frac{d\rho}{\rho} + \frac{du}{u} = 0 \quad \text{(Continuity)} \tag{2.2}$$

.

$$dp + \rho u du = 0 \quad \text{(Momentum)} \tag{2.3}$$

$$c_p dT - dq + u du = 0 \quad \text{(Energy)} \tag{2.4}$$

$$dp = d(\rho R T) \quad \text{(EOS)} \tag{2.5}$$

Let be the total mass flow rate combined from the first $(\dot{m}_{i_1})$ and secondary inlet $(\dot{m}_{i_2})$. The mass flow rate of the second inlet, $\dot{m}_{i_2}$, can be a function of the atmospheric velocity boundary layer which is defined as,

$$\dot{m}_{i_2} = 2\pi r (h_{c,i_2} - h_{c,i_1}) u_{i_2} \tag{2.6}$$

$$u_{i_2} = u_{ref} (\frac{h_{c,i_2}}{h_{ref}})^{\alpha} \tag{2.7}$$

where u_{ref} is the wind velocity measured at h_{ref} which is considered as the reference wind velocity value, and α is the wind shear exponent that can be calculated for small height differences as $\alpha = 1/ln(h_{ref}/h)$. However, in our calculations we considered the mass flow rate ratio, $\dot{m}_{i_2}/\dot{m}_{i_1}$ based on numerical results. The pressure drop correlations that were obtained for the collector and tower by considering the average value for c_p of air, and considering the average dimensional and field values for the collector$_{i1}$ and collector$_{i2}$ are as follows.

Collector pressure difference:

$$p_{c,o} - p_{c,i} \simeq \left[\frac{\dot{m}^2}{2\rho_{m,c}} \left(\frac{1}{A_{c,i}^2} - \frac{1}{A_{c,o}^2} \right) + \frac{q^{''}\dot{m}}{2\pi h_c^2 c_p \rho_{m,c} T_{m,c}} ln \frac{r_{c,i}}{r_{c,o}} \right] \tag{2.8}$$

Tower pressure difference for Manzanares case:

$$p_{t,o} - p_{t,i} \simeq -\rho_{m,t} g h_t \tag{2.9}$$

where $\rho_{m,c} - \rho_{m,t}$ are calculated by the average density values of air at inlet and outlet of collector and tower, by using Boussinesque approximation and lapse rate temperature change respectively. The ideal available power for the turbine is defined as

$$\dot{W} \simeq \frac{\dot{m}(p_{c,o} - p_{t,i})}{\rho_{turb}} \tag{2.10}$$

To calculate the turbine power for available pressure difference, the collector efficiency η_c was considered in our calculation as 0.32 based on reported values from Manzanares prototype.

$$P_t \;\; = \eta_c \dot{W} \tag{2.11}$$

4.2 Experimental Prodecure

To have a better understanding of SCPPS, and also benchmark our numerical results, an experimental study was conducted at a laboratory scale. Particle image velocimetry (PIV) was used to visualize and measure the velocity flow field in a small prototype (1/1000 scale of Manzanares prototype). The CFD analysis was performed for the laboratory prototype as well, for both types of collectors, traditional collector and the double-inlet collector. Fig. 2.5 shows the laboratory experimental arrangement.

A sensitive hotplate (1% K) was used to create the temperature gradient underneath the collector plate (70C for this experiment). The collector roof in the experimental model is height-adjustable via four aluminum legs attached to the edge of the collector plate. Fig. 2.6 shows the experimental apparatus, including the hot plate, chimney, camera, and laser and optical tools.

The flow field was illuminated with a Quantel Evergreen double-pulsed Nd:YAG laser (532 nm), operating at a frequency of 15 Hz, and the laser plane was oriented parallel to the collector, 3.96 mm above the hotplate. Images were taken using a LaVision SCMOS four-megapixel camera, located 0.762 m directly above the model. The entire setup including the hotplate, chimney, camera, and laser, were enclosed in a cage made of PVC pipe and 3 mm thick plastic sheeting. This was done to contain the glycol tracer particles in a large volume around the model.

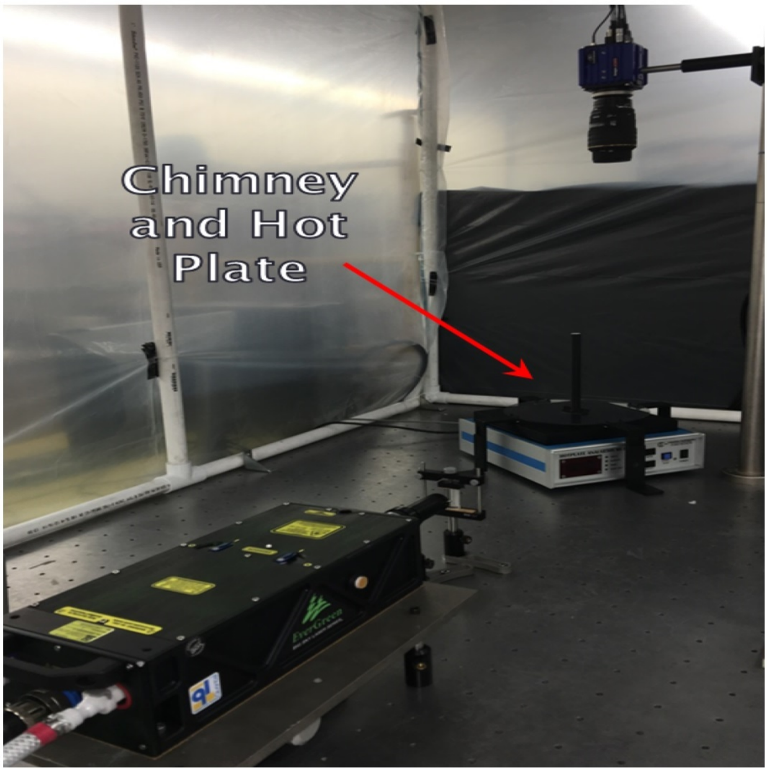

FIGURE 2.5: PIV SCPPS apparatus

5 Results and Disscusion

CFD simulations were performed for both cases A and B for a range of heat flux at the collector ground. Steady state numerical calculation was performed for both cases in an axisymmetric computational domain. To study the effect of available heat flux from the collector ground to the air on different field variables including temperature, density, pressure, and velocity, several calculations were performed for solar heat flux values q" of 400-1000 Wm^2 . All calculations were performed with second-order formal accuracy for all field variables. As mentioned before, for all mass, momentum and energy solutions, the residual convergence tolerance was set not to exceed 10^{-7}. As defined before, outlet mass flow rate is selected to calculate the iteration error values. The maximum relative iteration error, $e_{\dot{m}_i}$, is

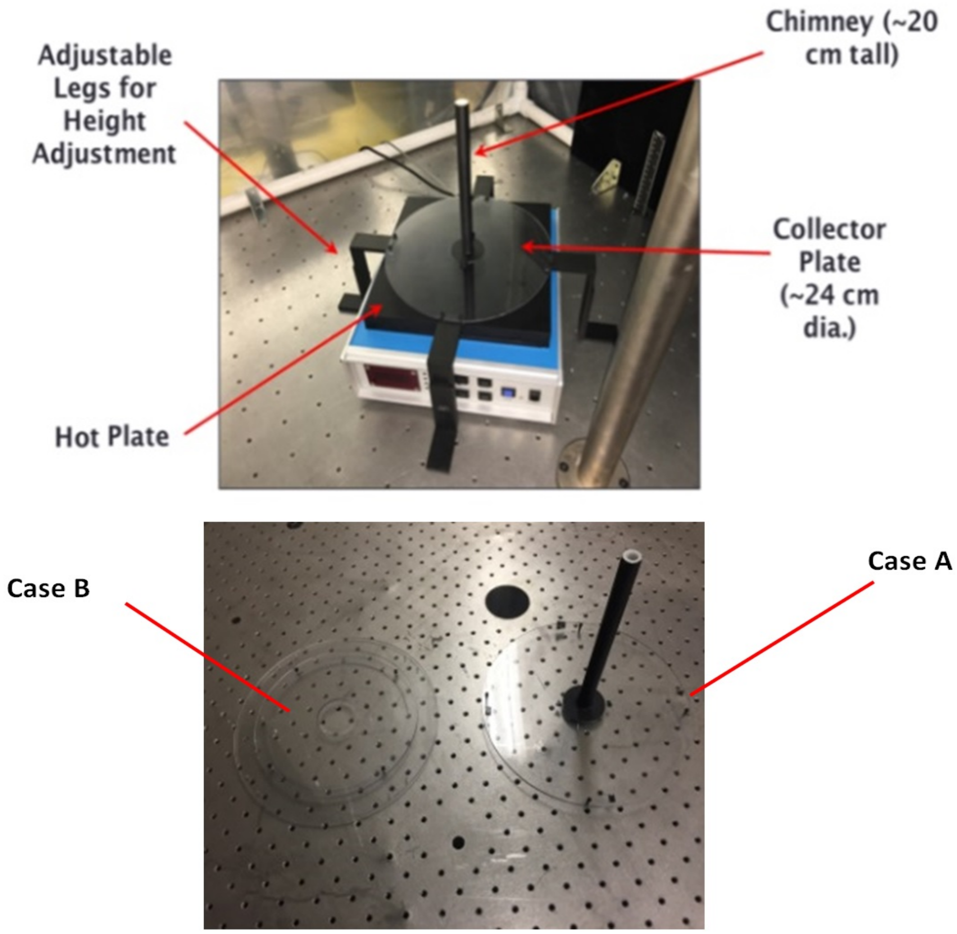

FIGURE 2.6: Collector and hot plate arrangement, two types of used collector in the experimental analysis

8.210^{-7} %. To study field variables quantitatively in the domain of SCPPS and perform post processing we obtained results in three regions (Fig. 2.7).

Air velocity in the collector is a function of its buoyancy and the geometry of the tower/collector. The driven buoyant air rotates the turbine which, in the majority of designs for SCPPS, is placed at the interface of the collector and tower (Fig. 2.7). Buoyant driven air velocity was captured along the collector from the spacing between two inlets until the axis of tower. In many articles, the reported velocity values are not a function of radiation or available heat flux at the collector. However, in our analysis the maximum velocity was obtained for

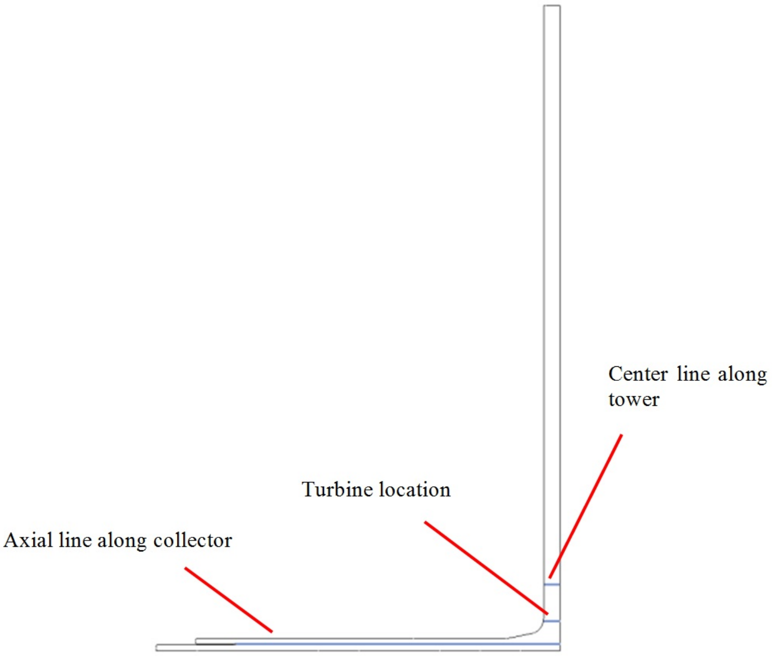

FIGURE 2.7: Location of probes for post processing

1000 W/m^2 and the minimum is for 400 W/m^2 (Fig. 2.8).

As shown in Fig. 4.8, the air velocity increases along the collector until reaching the chimney/tower interface. The maximum velocity is not at the axis due to the curve at the interface of the collector/tower and change of the air flow direction. However, along the tower the fully developed velocity is observed at a 20 m height (Fig. 2.9). As shown in Fig. 2.9 maximum velocity in all velocity profiles at this location for different heat flux values are located at the axis, $r = 0$.

As mentioned above, change of density plays a key role in this renewable power plant system. The density distribution along the collector is presented in Fig. 2.10. Maximum density is at the inlet collector location and minimum density occurs at the axis and the centerline of the collector. As it is apparent from Fig. 2.10, increasing in the heat flux leads to increase in the density variation along the

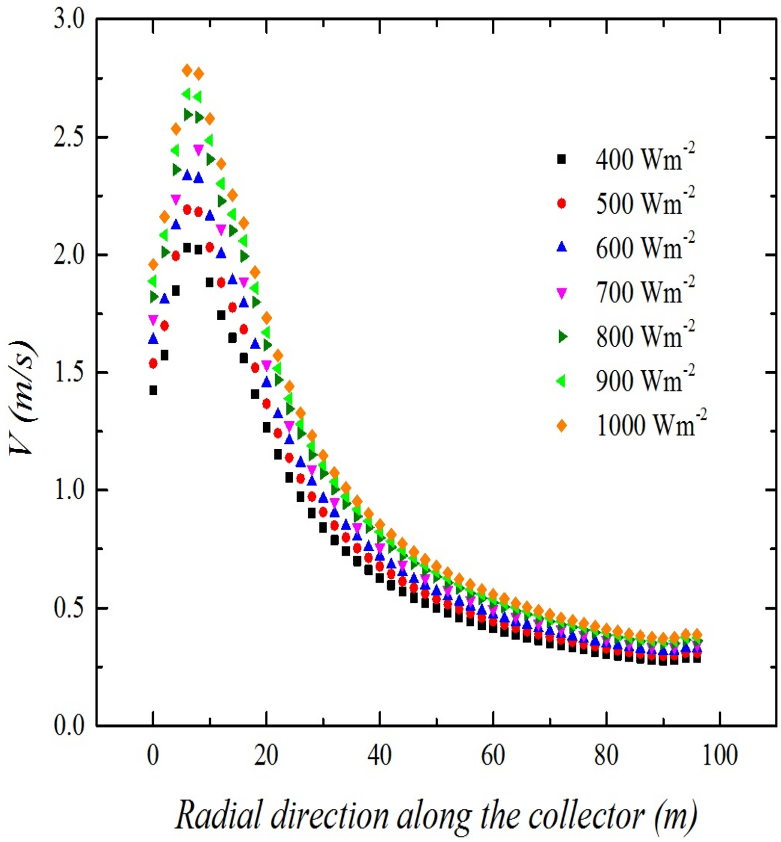

FIGURE 2.8: Velocity distribution along the collector for different heat flux values

collector. The evolution of pressure reduction due to density reduction is shown in Fig. 2.11.

In simulations pressure gauges were set to zero, and we just observe the effect of buoyancy effect to drive the flow, and have flow from upstream to downstream, which is the collector center. The total pressure as the sum of dynamic and static pressure is zero along the collector, leading to negative values for static pressure in the plot. Comparing this simulation with reality, we must note that we are ignoring the stack effect by setting the outlet pressure to zero as well.

Fig. 2.12 shows the temperature behavior along the collector probe line for different heat flux values. The maximum temperature for each profile occurs at

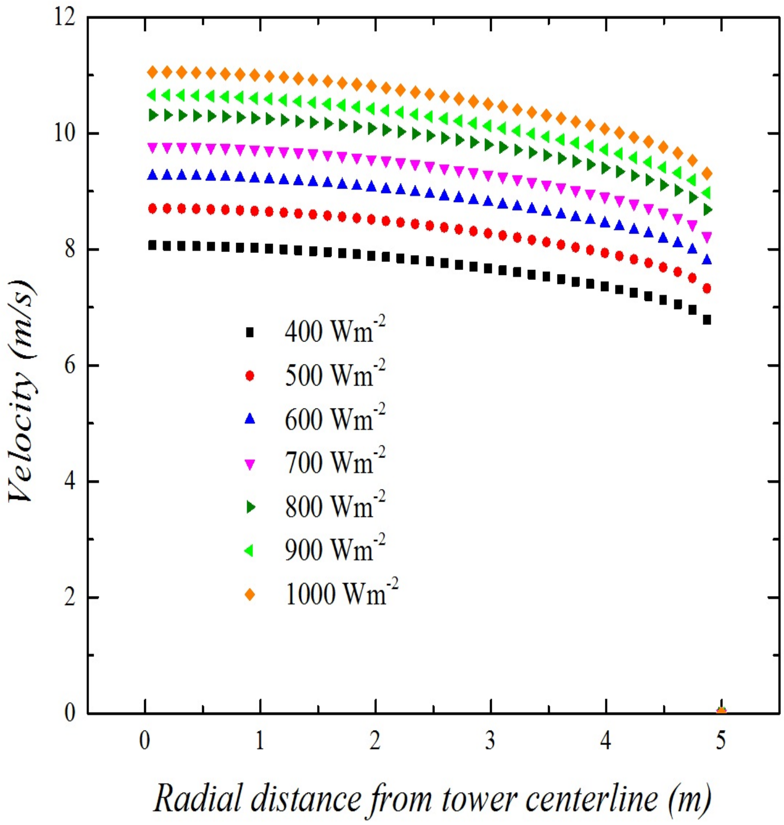

FIGURE 2.9: Velocity profile at 20 m of tower

the center zone of the collector: the bulk of air has achieved the maximum heat from the ground by passing through the collector which leads to the occurrence of the minimum density as shown in Fig. 2.10.

To calculate the available output power of SCPP, the velocity at the turbine location was considered. As shown in Fig. 2.13, the velocity profile is not fully developed yet. However, the maximum velocity occurs at the edge of turbine blades. The maximum available power based on the kinetic energy of air flow is $0.5\dot{m}u^2$. To have a more realistic approach we considered the reported turbine efficiency (85%) and calculated 2/3 of the remained energy. In the case of an enclosed turbine, it is a conservative estimate which can also be considered to account for internal turbine conversion losses.

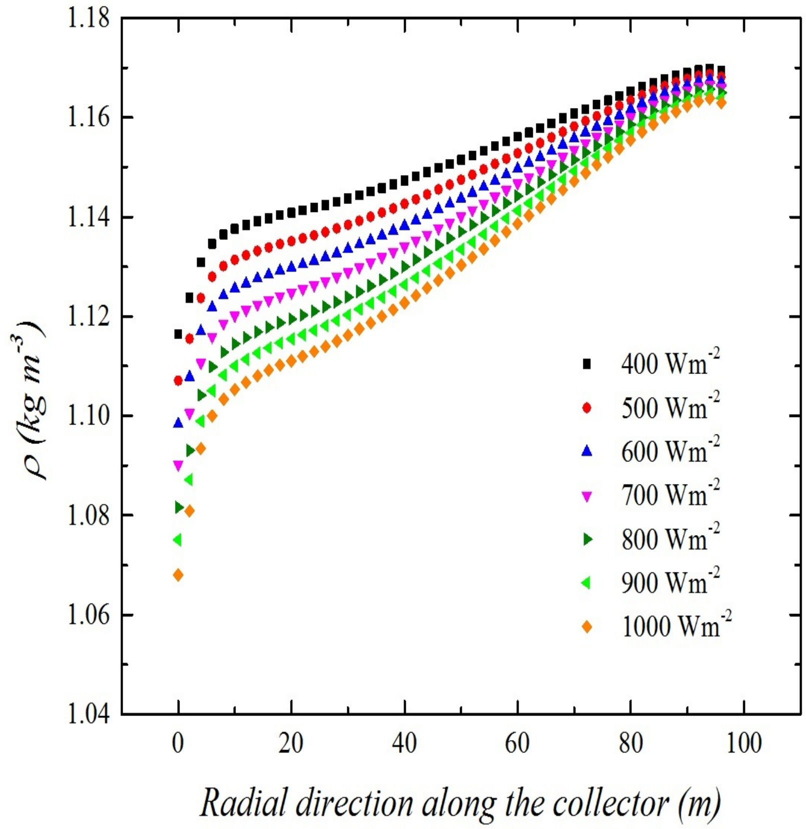

FIGURE 2.10: Density distribution along the collector

The output power from case B was calculated from CFD results and analytical correlations (Fig. 2.14). It appears that for double-inlet collector the output power increases about 14% in comparison with single-inlet. As heat flux increases, we observe reduction in power increase in case B (double-inlet collector) due to the air back-flow/return from the collector to ambient condition. Return mass flow increases after 800 W/m^2 due to the greater temperature difference of air inside of the collector close to the inlet zone and the ambient temperature.

It is obtained that the characteristics of double-inlet SCPPS is not the same as single-inlet and back flow occurs for a lower heat flux. Analytical approach for case B gives us higher power output due to ignoring the back-flow effect, and several simplifications in this one-dimensional analysis, including using average values for

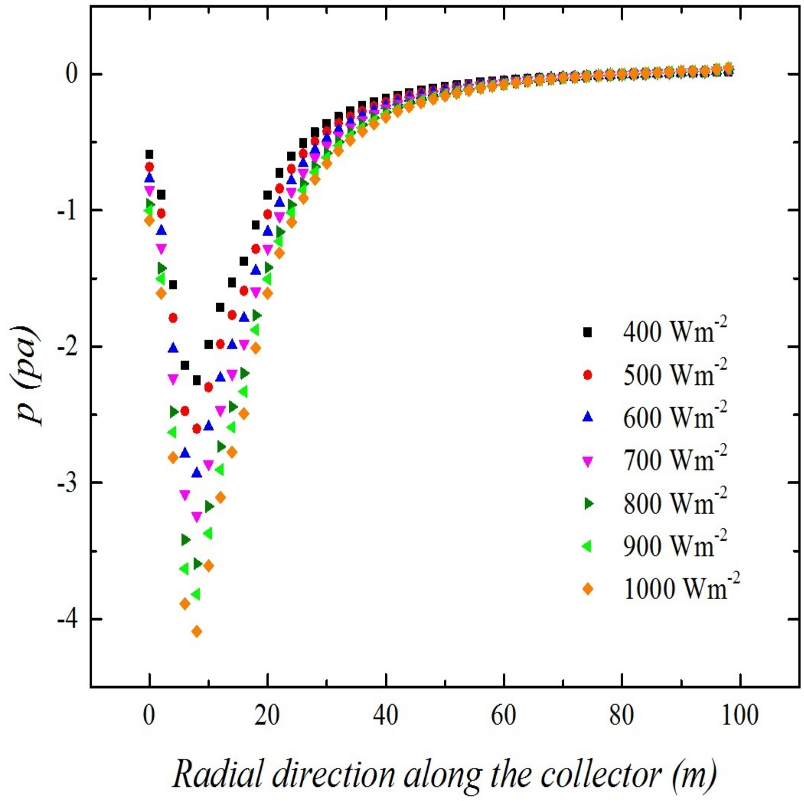

FIGURE 2.11: Pressure evolution along the collector

density, temperature. Also in the analytical-correlation the friction is neglected in the derived PDEs. However, we have considered the same collector efficiency factor to have a more realistic approach in our analytical model. To evaluate our numerical analysis more quantitatively, a small modular SCPPS was fabricated to perform PIV measurements. Hot plate plays the same role as irradiated collector ground which provides heat to the air and generates buoyancy-driven air flow. The velocity field was evaluated and measured to calculate the total mass flow rate and the updraft velocity. Mass flow rate and therefore average updraft velocity is the system response quantity (SRQ) in our validation analysis. Several experiments were performed for different cases; however, in this article we are presenting the results for the single inlet collector validation metric analysis. Fig. 2.15 presents

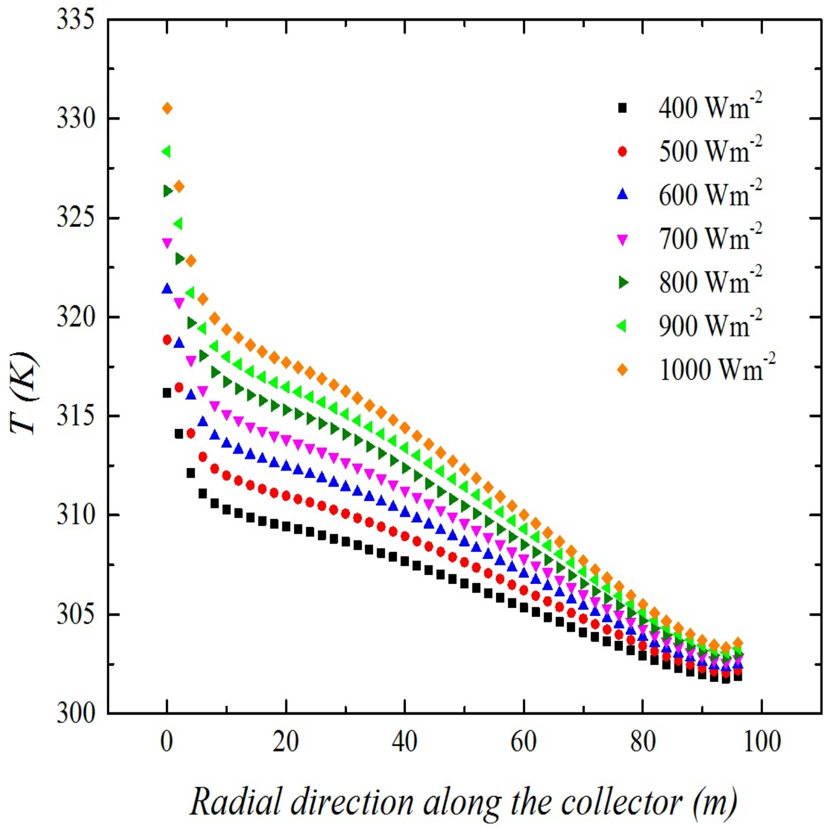

FIGURE 2.12: Temperature distribution along the collector

the region of interest to measure the velocity in the small SCPPS. Several simulations were performed for this prototype similarly to the large-scale, Manzanares system. The epistemic uncertainty of the applied grids was quantified by GCI study as a part of our solution verification.

The iteration error was 100 times smaller than grid uncertainty and we did not include them in our error uncertainty calculation. To perform validation, error is defined as, $E = S - D$ [19]. The experimental data was considered as the reference of error. However, the uncertainty of error includes the uncertainty of the simulation based on epistemic uncertainty observed by solution verification. Validation model assessment was performed by using modified area validation metric [20, 21].

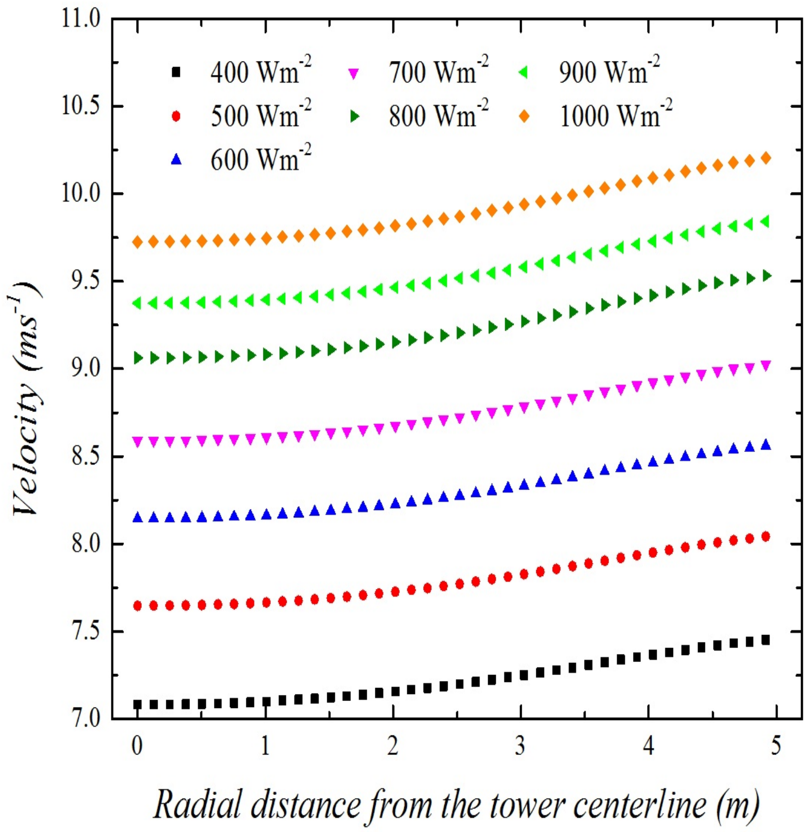

FIGURE 2.13: Velocity distribution at the turbine location

The cumulative and empirical probabilities of the system of response quantity from experimental measurements and from simulation results were observed. The quantitative mismatch of cumulative distribution of experimental data and empirical distribution function (EDF) of simulation results of SRQ, which called validation metric area (d), were calculated. Fig. 2.16 is the EDF/CDF representation of cumulative experimental and numerical results.

The colored areas are the mismatch of experimental and simulation cumulative values. Red area presents the positive mismatch (d^+) and blue area presents the negative mismatch (d^-) which is counted to calculate the model error uncertainty, u_{model}. The validation standard uncertainty, u_{val}, which is defined as the summation of all uncertainties as input uncertainties and experimental uncertainties.

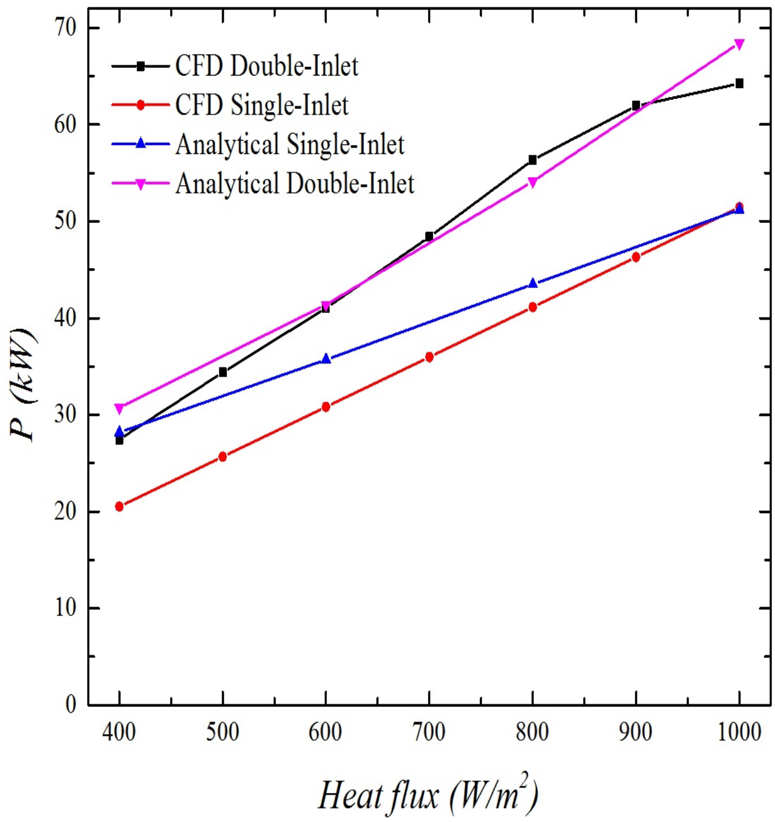

FIGURE 2.14: Output power for different cases

In our analysis, we have just considered u_{model} and did not have values for the other uncertainties. Therefore, the validation standard uncertainty u_{val} in our simulation is the same as u_{model}. The validation metric which is E and u_{val} can be correlated by using a factor of safety and define an interval which u_{val} falls in with a defined confidence level. The chosen confidence level based on reported $V\&V20$ standards is 95%.

$$u_{model} = [S - F_s d^-, S + F_s d^+] = [8.15, 10.3] mm/s \tag{2.12}$$

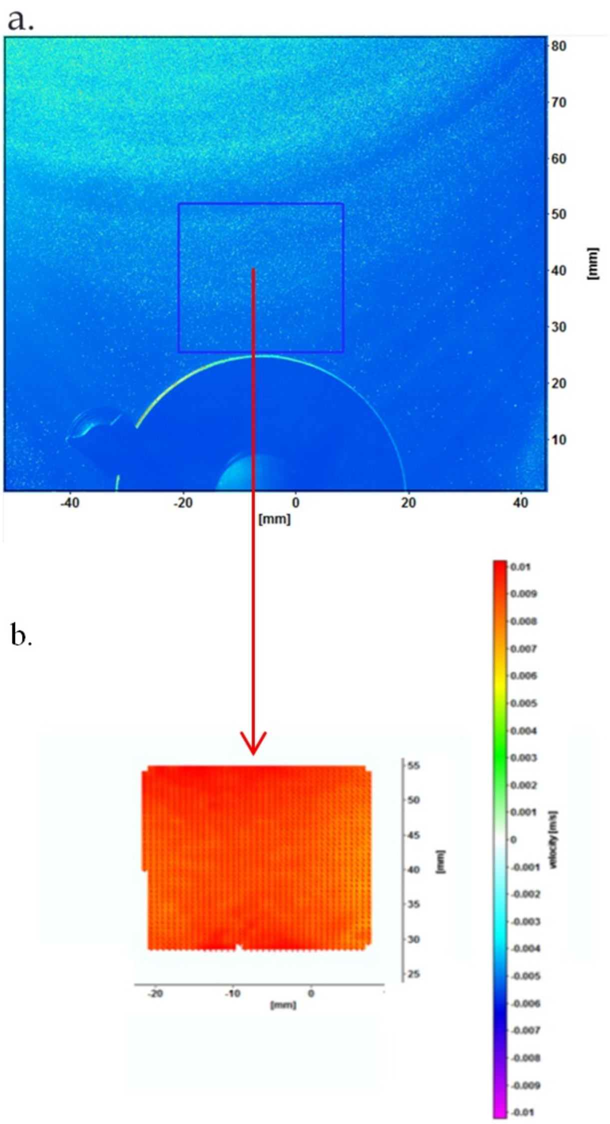

FIGURE 2.15: Experimental region of interest, blue Square (a) and averaged velocity vector/contour plot of the area of interest (b)

2.6 Conclusion

Double-inlet collector design for SCPPS was presented and evaluated against the traditional collector design. Computational analysis for different cases was conducted to evaluate this idea. For Manzanares prototype applying double-inlet collector design increases the overall efficiency up to 14%. One-dimensional analytical study for double-inlet collector also was conducted and compared against

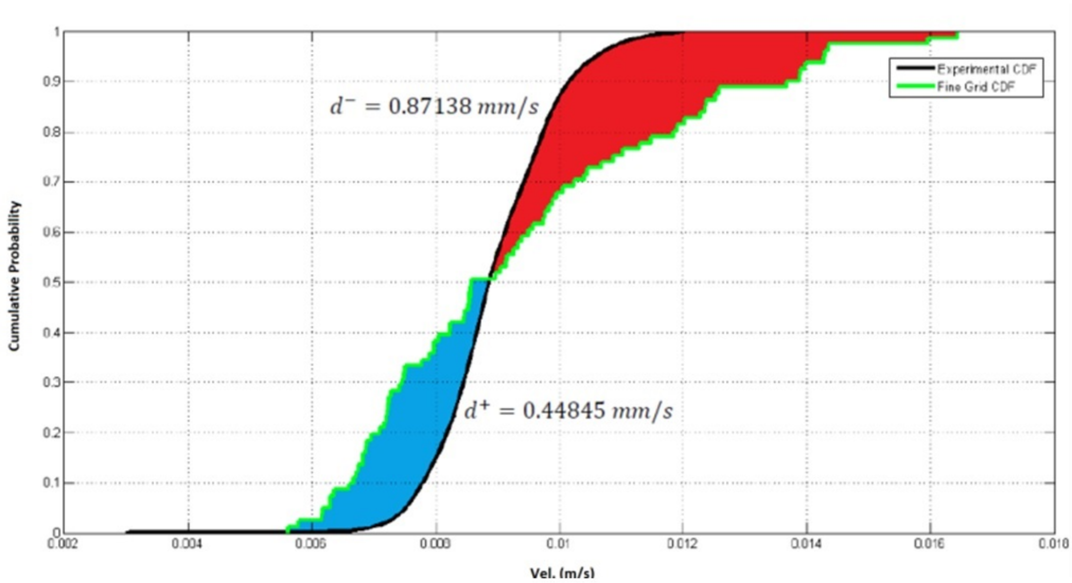

Figure 2.16: Cumulative probabarity of D and S, area metric validation representation

the CFD results for traditional and the proposed design. In the analytical study with respect to ignoring the backflow effect, the agreement of results decreases by increasing the available heat flux. PIV analysis was performed to have a better understanding on SCPPS air flow for a smaller prototype. Validation metric study was performed for this prototype to evaluate the fidelity our CFD model. The validation standard uncertainty of model was obtained for the smaller prototype.

References

[1] Crabtree, George W., and Nathan S. Lewis. "Solar energy conversion." Physics today 60, no. 3 (2007): 37-42.

[2] Haaf, W., K. Friedrich, G. Mayr, and J. Schlaich. "Solar chimneys part I: principle and construction of the pilot plant in Manzanares." International Journal of Solar Energy 2, no. 1 (1983): 3-20.

[3] Bernardes, MA dos S., A. Voß, and G. Weinrebe. "Thermal and technical analyses of solar chimneys." Solar Energy 75, no. 6 (2003): 511-524.

[4] Bonnelle, Denis. "Solar chimney, water spraying energy tower, and linked renewable energy conversion devices: presentation, criticism and proposals." PhD, University Claude Bernard-Lyon (2004).

[5] dos Santos Bernardes, Marco Aurelio, Ramon Molina Valle, and Márcio Fonte-Boa Cortez. "Numerical analysis of natural laminar convection in a radial solar heater." International journal of thermal sciences 38, no. 1 (1999): 42-50.

[6] Schlaich, Jorg, Rudolf Bergermann, Wolfgang Schiel, and Gerhard Weinrebe. "Design of commercial solar updraft tower systems—utilization of solar induced convective flows for power generation." Journal of Solar Energy Engineering 127, no. 1 (2005): 117-124.

[7] Fathi, Nima, Patrick Mckdaniel, Seyed Sobhan Aleyasin, , Matthew Robinson, Peter Vorobieff, Salvador Rodriguez, and Cassiano de Oliveira. "Improving the Efficiency of the Solar Chimney Power Plant by Use of Waste Heat from Power Plants (Nuclear and Conventional)." Journal of Cleaner Production (2017).

[8] Pretorius, Johannes Petrus. "Optimization and control of a large-scale solar chimney power plant." PhD diss., Stellenbosch: University of Stellenbosch, 2007.

[9] Betz, Albert. Introduction to the theory of flow machines. Elsevier, 1966.

[10] Pasumarthi, N., and S. A. Sherif. "Experimental and theoretical performance of a demonstration solar chimney model—Part I: mathematical model development." International Journal of Energy Research 22, no. 3 (1998): 277-288.

[11] P. Vorobieff, A. Mammoli, N. Fathi, V. Putkaradze , “Free-standing inflatable solar chimney: experiment and theory,” American Physical Society Division of Fluid Dynamics, San Francisco, CA, 2014.

[12] Putkaradze, Vakhtang, Peter Vorobieff, Andrea Mammoli, and Nima Fathi. "Inflatable free-standing flexible solar towers." Solar Energy 98 (2013): 85-98.

[13] Schlaich, Jörg. The solar chimney: electricity from the sun. Edition Axel Menges, 1995.

[14] Fluri, T. P., and T. W. Von Backström. "Performance analysis of the power conversion unit of a solar chimney power plant." Solar Energy 82, no. 11 (2008): 999-1008.

[15] Denantes, F., and E. Bilgen. "Counter-rotating turbines for solar chimney power plants." Renewable energy 31, no. 12 (2006): 1873-1891.

[16] Fluri, T. P., and T. W. Von Backström. "Comparison of modelling approaches and layouts for solar chimney turbines." Solar Energy 82, no. 3 (2008): 239-246.

[17] "Annular Flow Convection Chimney (AFCC), Multi Inlet Solar Thermal Array Collector-Tower" Nima Fathi, Peter Vorobieff, Seyed Sobhan Aleyasin and Andrea Mammoli . (2015) Flintbox.
http://www.flintbox.com/public/project/29725/

[18] Fathi, Nima, Seyed Sobhan Aleyasin, and Peter Vorobieff. "Numerical–analytical assessment on Manzanares prototype." Applied Thermal Engineering 102 (2016): 243-250.

[19] Oberkampf, William L., and Christopher J. Roy. Verification and validation in scientific computing. Cambridge University Press, 2010.

[20] Voyles, Ian T., and Christopher J. Roy. "Evaluation of model validation techniques in the presence of aleatory and epistemic input uncertainties." In 17th AIAA Non-Deterministic Approaches Conference, p. 1374. 2015.

[21] Voyles, Ian T., and Christopher J. Roy. "Evaluation of Model Validation Techniques in the Presence of Uncertainty." In 16th AIAA Non-Deterministic Approaches Conference, p. 0120. 2014.